Il presente lavoro è stato pubblicato su Microporous and Mesoporous Materials 212, 2015, 35-47 con doi
http://dx.doi.org/10.1016/j.micromeso.2015.03.012

Synthesis of zeolites at low temperatures in fly ash-kaolinite mixtures

Claudia Belviso [a, *], Lorena C. Giannossa [b], F. Javier Huertas [c], Antonio Lettino [a], Annarosa Mangone [b], Saverio Fiore [a]

[a] *Institute of Methodologies for Environmental Analysis, National Research Council of Italy (IMAA-CNR), Tito Scalo, Potenza, Italy*
[b] *Department of Chemistry, University Aldo Moro, Bari, Italy*
[c] *Instituto Andaluz de Ciencias de la Tierra - IACT (CSIC-University of Granada), Armilla, Granada, Spain*

* Corresponding author. Tel.: þ39 0971427224; fax: þ39 0971427222, *E-mail address:* claudia.belviso@imaa.cnr.it (C. Belviso).

ABSTRACT

Coal fly ash from an Italian coal-fired power plant, kaolinite from the Source Clay Repository of The Clay Minerals Society, and four derived mixtures were used to synthesize zeolite using hydrothermal treatment at 45 °C in distilled water after alkaline fusion. The results documented that geopolymers,
A-type and X-type zeolites were formed in different quantities, depending on the starting material and the duration of the experiment. Zeolite-X was the prevailing phase synthesized using pure fly ash, zeolite-A formed in higher amounts from kaolinite, and comparable amounts of A- and X-type zeolites crystallized, thereby adding 20 and 40% kaolinite to the fly ash, respectively. Zeolite-A as main phase was synthesized already adding 60% or even up to 80% kaolinite to the fly ash. Sodalite occasionally formed from the source materials, whereas zeolite ZK-5 was synthesized from only fused fly ash (100FA). The data indicated that, in addition to the Si/Al ratio of solid source materials, zeolite formation was controlled by the time and chemistry of the solution. The polymerization of alumina-silicate gels changed during the experiments, likely due to the amorphization of metastable zeolites.

1. Introduction

Zeolites are hydrated aluminosilicate minerals that can be synthesized using several source materials, such as fly ash (e.g., [1-11]) and kaolinite (e.g., [12-19]). Experiments using fly ash have been performed with a hydrothermal reaction in alkaline solutions (e.g., [3,4]) and after a fusion pre-treatment (e.g., [9-11]). Microwaves (e.g., [20,21]) and ultrasonic treatments (e.g., [22-26]) have been employed to increase kinetic reactions. The use of kaolinite generally requires calcination at high temperatures (600e1000 °C), and only a few recent studies have introduced pre-fusion treatment with alkalis [17,19,27] or hydrothermal treatment with an NaOH solution [28]. In spite of several papers detailing the synthesis of zeolites using kaolinite or fly ash, there are aspects that are not fully understood. The most relevant

aspects are related to the role of Si/Al in the starting material, the crystallization time and temperature and the incubation time. Different literature indicates that zeolite- A was formed with a molar ratio of Si/Al >2 (e.g., [29,30]) or Si/Al < 2 (e.g., [19,31-33]), whereas the zeolite-X was synthesized with pre-fusion at an incubation temperature < 60 °C (e.g., [9-11]) or > 60 °C (e.g., [6]). In terms of the crystallization time, various authors synthesized zeolite-A between 8 and 24 h [34] or after 96 h (e.g., [19]).

In a previous study [19], we documented that the use of almost pure kaolinite is mainly conducive to zeolite-A and to traces of zeolite-X, but if minor amounts of other silicate minerals (e.g., illite and quartz) are associated with kaolinite, the quantity of zeolite-X significantly increases. It has also been ascertained [11] that the presence of Mg and Ca in the contact solution plays a determinant role in the formation of zeolite-X. In addition to the chemical composition of the starting material and the contact solution, the incubation time may favour the crystallization of one type of zeolite with respect to another one (e.g., [35]); furthermore, it has been suggested [11] that the crystallization rates of zeolite-A and zeolite-X change over time. To provide more information about the role of Si/Al and time in controlling the hydrothermal synthesis of zeolites after fusion with NaOH, we performed new experiments by fixing the temperature at 45 °C and ageing a coal fly ash, a pure kaolinite, and four mixtures of these two materials in distilled water for 1-216 h.

2. Materials and methods

The experiments were performed with coal fly ash (FA) from an Italian thermoelectric power plant that we have used in previous experiments [9-11,25,26] and kaolinite (KGa-2) from the Source Clay Repository of The Clay Minerals Society. These two materials had a similar Si/Al ratio (FA:1.46; KGa-2:1.01), and therefore it changed little in the four mixtures (Table 1). The major element chemical analyses were performed on pressed powder pellets using X-ray fluorescence spectrometry (XRF; Philips PW 1480). It was used a Cr anode tube at 60 kV and 50 mA. The loss on ignition (LOI) was measured by heating the sample at 900 °C for 3 h. The mineralogical composition was determined by powder X-ray diffraction (XRD) using a Rigaku Rint 2200 diffractometer equipped with Cu-Kα radiation (40 kV and 30 mA) and a graphite monochromator. The data collections were performed in the 2θ range 2-54° with step size of 0.02°.

The morphological features of the starting and aged materials were observed using a field emission scanning electron micro- scope (SEM, Zeiss Supra 40). The samples were carbon-sputtered (10 nm thick) in order to avoid charging of the surface. Elemental analyses were performed with an energy-dispersive X-ray spectrometer (EDS, Oxford Inca Energy 350) equipped with a Si(Li) detector.

The starting materials were fused using NaOH (1:1.2 weight ratio) and, with distilled water added,

were stirred overnight at room temperature. The suspensions were incubated at 45 °C for 1, 6, 12, 24, 48, 72, 96, 120, 144, 168, 192, and 216 h in separate experiments. The incubation temperature was chosen based on our previous studies [9,10,19], which indicated that a large amount of zeolites formed at 45 °C from fly ash or kaolinite. The solids and solutions were then separated by centrifugation.

The solids were washed with distilled water, dried in an oven at 30 °C and characterized using SEM and XRD. Quantitative mineralogical analyses were not reliable because of the presence of high amount of non-crystalline materials (mainly neoformed geopolymers) that continuously changed their polymerization state during the incubation time. An estimation of each neo-formed mineral in the different experiments was performed by

comparing the integrated intensities of the selected XRD diffraction lines (X-type zeolite: I_{111} at 6.09° 2 θ; A-type zeolite: I_{222} at 7.20° 2 θ; sodalite: I_{110} at 13.92° 2 θ; zeolite ZK-5: I_{200} at 9.30° 2 θ).

The solutions were analysed for Si, Al, Ca, Mg, Na, and K contents using an inductively coupled plasma mass spectrometer (ICP-MS; Perkin Elmer ELAN 9000). Analytical precision was better than 5% except for Ca (<10%).

To obtain information regarding the coordination state of aluminium, the two starting materials (FA and KGa-2) and their fused products (100FA and 0FA) were analysed with a solid state nuclear magnetic resonance spectrometer (Bruker Avance I 400 MHz) using a magic angle spinning technique (MAS-NMR).

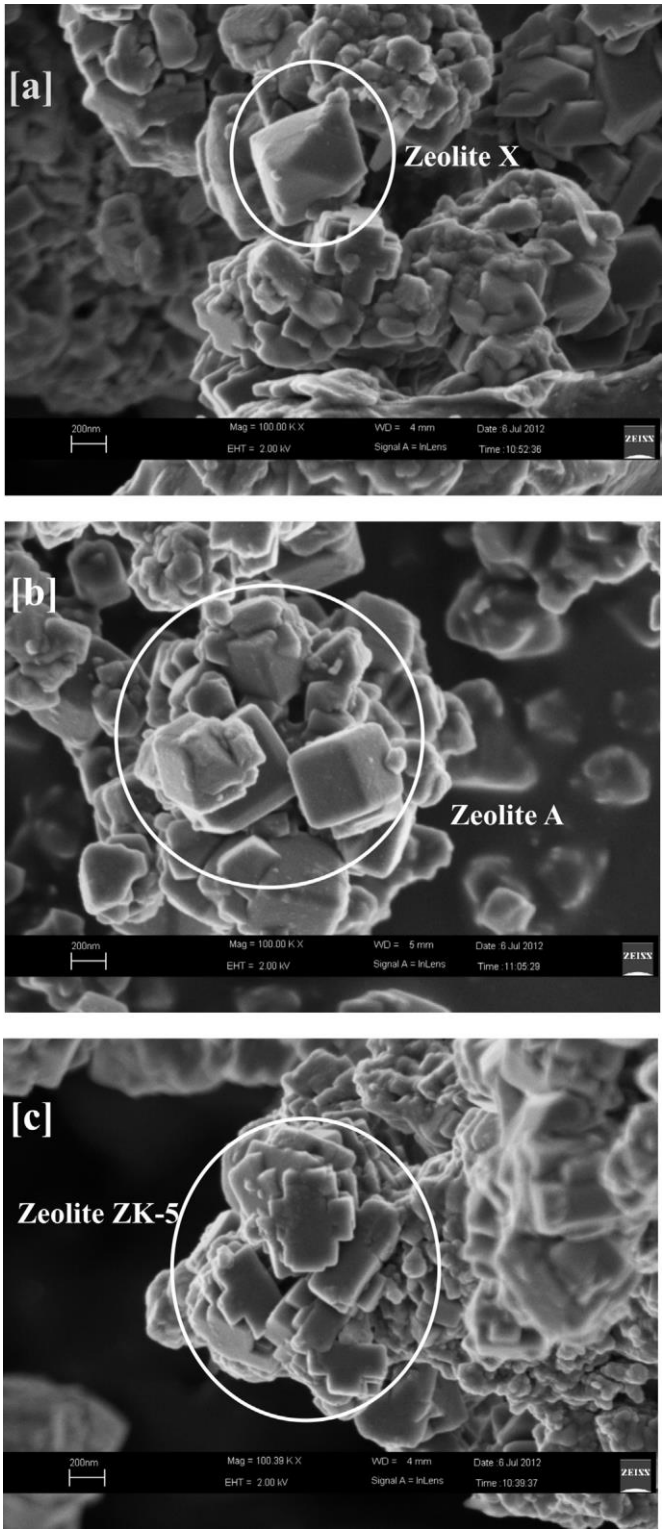

Fig. 1. Selected SEM images of zeolites synthesized using mixtures of fly ash and kaolinite after 48 h of incubation. [a] octahedral crystals of X-type zeolite (40FA sample); [b] cubic crystals of A-type zeolite (0FA sample); [c] typical morphology of zeolite ZK-5 (100FA sample).

Table 1 Mixtures of FA and KGa-2. Si/Al = molar ratio.

Mixture	FA	KGa-2	Si/Al
100FA	100	0	1.46
80FA	80	20	1.35
60FA	60	40	1.25
40FA	40	60	1.16
20FA	20	80	1.08
0FA	0	100	1.01

Si/Al: determined in FA and KGa-2 samples; “calculated” in the mixtures.

Table 2 Specific integrated intensities measured on 100FA, 0FA and 4 mixtures at different incubation time.

	Zeolite	Time (hours)												
		1	6	12	24	48	72	96	120	144	168	192	216	
100FA	ZeoX	-	-	32	137	120	112	80	152	81	108	**190**	167	Si/Al = 1.46
	ZeoA	-	-	-	-	-	-	-	-	-	-	-	-	
	Sod	29	29	35	-	**125**	77	61	78	107	101	-	-	
	ZK5	-	-	52	-	**234**	177	329	-	180	104	-	-	
80FA	ZeoX	234	269	**284**	250	153	194	143	130	140	200	168	188	Si/Al = 1.35
	ZeoA	-	-	30	**120**	102	90	78	50	-	15	43	57	
	Sod	-	-	-	-	-	-	-	38	**76**	32	29	31	
	ZK5	-	-	-	-	-	-	-	-	-	-	-	-	
60FA	ZeoX	247	**262**	175	139	134	213	130	100	149	115	150	150	Si/Al = 1.25
	ZeoA	-	54	107	**205**	113	154	79	60	141	79	92	114	
	Sod	-	41	-	-	-	-	134	32	-	**152**	99	28	
	ZK5	-	-	-	-	-	-	-	-	-	-	-	-	
40FA	ZeoX	94	59	**145**	85	116	85	91	75	85	99	69	120	Si/Al = 1.16
	ZeoA	-	39	150	260	213	**349**	186	181	293	287	270	137	
	Sod	-	-	27	-	-	-	-	-	11	13	-	**127**	
	ZK5	-	-	-	-	-	-	-	-	-	-	-	-	
20FA	ZeoX	104	**337**	48	35	21	27	26	39	48	58	22	40	Si/Al = 1.08
	ZeoA	100	152	205	412	301	**435**	235	382	364	394	337	132	
	Sod	13	-	-	-	-	-	-	-	9	11	25	**307**	
	ZK5	-	-	-	-	-	-	-	-	-	-	-	-	
0FA	ZeoX	-	-	**20**	-	-	25	-	-	-	-	-	-	Si/Al = 1.01
	ZeoA	-	-	148	519	537	500	611	591	586	576	322	575	
	Sod	311	**324**	-	-	-	-	-	-	-	41	74	-	
	ZK5	-	-	-	-	-	-	-	-	-	-	-	-	

ZeoX = X-type zeolite; ZeoA = A-type zeolite; Sod = sodalite; ZK5 = zeolite ZK-5. The highest values are shown in bold.

3. Results

3.1. SEM observations

The SEM observations (Fig. S1) (see Supporting Information) confirmed that the coal fly ash was mainly composed of spherical particles of variable size, from some tens of nanometres to about one hundred micrometres. Occasionally, glass shards and unburned coal grains were also observed. The kaolinite

crystals exhibited pseudo-hexagonal outlines with highly variable dimensions (from less than 300 nm to several micrometres).

The SEM observations of the samples after incubation revealed the presence of zeolites with different morphologies. The most frequent zeolite observed was the X-type, which displayed the typical octahedral morphology (Fig. 1a), and the A-type, which was characterized by cubic outlines (Fig. 1b). The sizes of both morphological types were homogeneous (200–400 nm), and they frequently formed both homotypic and heterotypic aggregates. In some experiments involving 100FA, there were crystals showing morphologies ascribable to zeolite ZK-5 (Fig. 1c), whose presence was confirmed by XRD analyses.

3.2. XRD analysis

The XRD patterns of the starting materials and their incubated products are reported in Fig. S2 and Fig. S3-S4, respectively. The integrated intensities of the selected diffraction lines of the zeolites, which can provide better information about the amount formed from given starting materials at different times, are reported in Table 2. Calcite was detected in all of the samples in decreasing amounts, from 100FA to 0FA, as a function of the initial Ca content of the starting material.

Fly ash and kaolinite. The patterns of FA and KGa-2 are reported in Fig. S2. The FA was mostly composed of amorphous alumino- silicates; however, mullite and quartz were present in low amounts. As expected, the KGa-2 was composed of poorly crystalline kaolinite with traces of anatase.

100FA and 0FA. Fig. S3 indicates the XRD profiles of the fused fly ash (100FA) and the fused kaolinite (0FA) samples after incubation. In the 100FA, X-type zeolite formed beginning at 12 h (Fig. S3a); however, the amount decreased during incubation for 96 h. Zeolite ZK-5 was present in the experimental products at 12, 48, 72, 96, 144, and 168 h, but it was not detected in the other experiments. Sodalite was the sole zeolite formed during shorter incubation times (1 and 6 h), and it crystallized in variable amounts in all of the other products. It was not found in the samples incubated for 24, 192, and 216 h. The X-ray profiles of kaolinite (0FA) indicated that A-type zeolite was the main newly formed phase starting from 12 h; X-type zeolite was present in very low amounts after 12 h (Fig. S3b). During shorter incubation times (1 and 6 h), only sodalite formed; this mineral was also detected in the products incubated for 168 and 192 h.

80FA Mixture. The XRD patterns of these samples (Fig. S4a) indicate the crystallization of X-type zeolite beginning after 1 h, whereas the A-type zeolite formed after 12 h, and the amount present changed significantly over time. The amount of X-type zeolite tended to decrease as the incubation time increased, whereas an irregular trend was detected for A-type zeolite. Sodalite formed after 120 until 216 h.

Table 3 XRF analysis of fly ash and kaolinite samples.

Major elements (wt.%)	F1	KGa-2
SiO_2	48.47	44.60
Al_2O_3	28.03	37.48
Fe_2O_3	4.38	1.20
TiO_2	1.45	2.30
MnO	0.08	n.d.
MgO	1.36	n.d.
CaO	6.38	0.01
Na_2O	0.49	0.01
K_2O	0.94	0.04
P_2O_5	0.44	0.04
LOI	7.98	14.30

n.d. Not detected.

60FA Mixture. XRD analysis of the 60FA mixture (Fig. S4b) indicated that zeolite-X was the only phase formed after 1 h, but its amount decreased over time. Conversely, the amount of zeolite-A began to increase after 6 h. Sodalite formed after 6 h; it then disappeared after longer incubation times and crystallized again after 96 h until the end of the experiment.

40FA Mixture. The XRD patterns of the 40FA mixture (Fig. S4c) indicated that the formation of zeolite-X began after 1 h of incubation, but its amount decreased after 24 h until 120 h and then increased until 216 h. Zeolite-A formed after 6 h and increased in amount after 12 h until the end of the incubation. Small amounts of sodalite were synthesized after 12, 144, 168 h; during the longest incubation (216 h), the amount of sodalite significantly increased.

20FA Mixture. The XRD profiles of 20FA (Fig. S4d) showed significant variation in the amount of zeolites formed during the short incubation times. After 1 h, the diffraction lines of A- and X-type zeolites were quite comparable. After 6 h, zeolite-X was the primary newly formed mineral. From 12 h until the end of the experiment, a larger amount of zeolite-A formed, whereas the amount of zeolite-X significantly decreased. Sodalite was detected after incubation for 1 h and then again after 168 h until the end of the experiment.

3.3. MAS-NMR analysis

^{27}Al MAS NMR spectra are shown in Fig. S5. As expected, the spectrum recorded on KGa-2 contained a sole intense signal that shifted very close to 0 (at approximately 1.5 ppm) and was due to octahedral AlO^{VI}. On the contrary, the fly ash exhibited a number of very low-intensity peaks, indicating that the Al existed in different chemical environments. The spectra of the fused products were very distinct from those of the pristine materials: the 0FA sample was characterized by the presence of an intense signal

ascribable to Al^{IV} (63.8 ppm) and by a very weak signal that shifted to 15 ppm due to octahedral aluminium. It should be noted that this latter signal was different from the AlO^{VI} signal recorded on KGa-2,

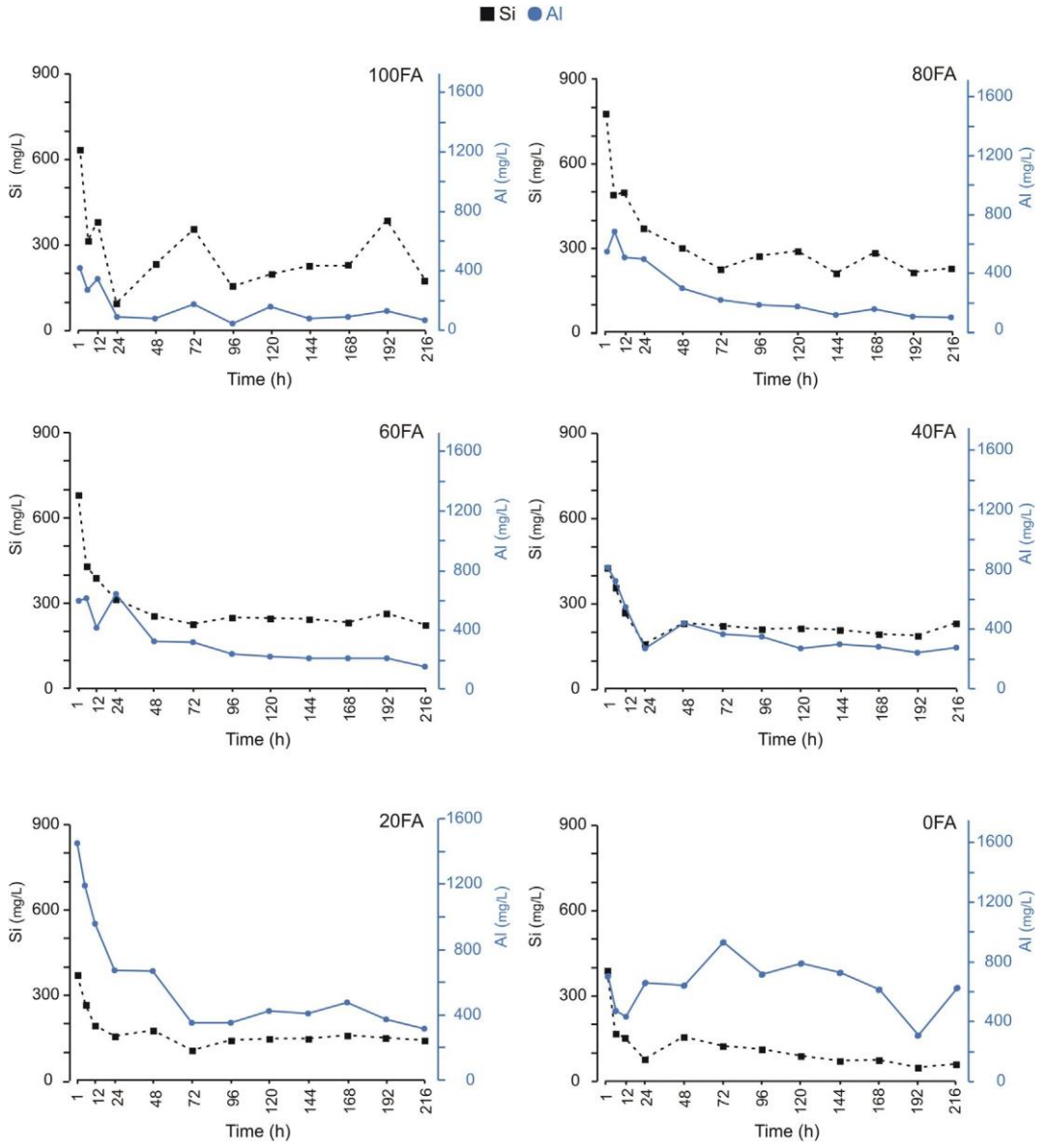

Fig. 2. Evolution of the Si and Al concentrations (mg/L) in the supernatant solutions over time.

thereby indicating, in accordance with XRD data, that the crystalline structure of kaolinite collapsed after alkaline fusion. The 100FA sample exhibited an intense peak at 63.7 ppm due to tetra-coordinated aluminium.

3.4. XRF analysis

The chemical compositions (major elements) of the FA and KGa- 2 are reported in Table 3. The silica contents of both samples were comparable (approximately 49% and 45% in FA and KGa-2, respectively), but the amount of alumina was higher in the KGa-2 (=38%) than in the FA (=26%). The difference in the Al content led to a slight difference in the Si/Al molar ratios (0.45; Table 1). The Fe_2O_3, MgO, CaO, Na_2O and K_2O contents were higher in the FA, whereas the TiO_2 content was lower (1.45% and 2.30% in FA and KGa-2, respectively).

3.5. ICP-MS analysis

The Si and Al concentration in the supernatant solutions after incubation at different times are reported in Table S1 and in Fig. 2. In detail, in the 100FA, the Si_{aq} and Al_{aq} tended to an exponential decrease but over longer times their concentrations increased and later remained almost constant. The 80FA, 60FA, 40FA and 20FA contact solutions were characterized by a generally exponential decreasing trend. A sensible Al_{aq} variation was detected in the 60FA and 40FA solutions after 24 h of incubation, increasing to 637 mg/L and decreasing to 271 mg/L, respectively. 0FA was characterized by a weak decreasing trend in Si_{aq} and variable behavior of Al_{aq}, with the highest (928 mg/L) and lowest (306 mg/L) values after 72 and 192 h of incubation, respectively. However, the Al concentration in the supernatant solutions was generally higher than the Si concentration in the 40FA, 20FA and 0FA contact solutions.

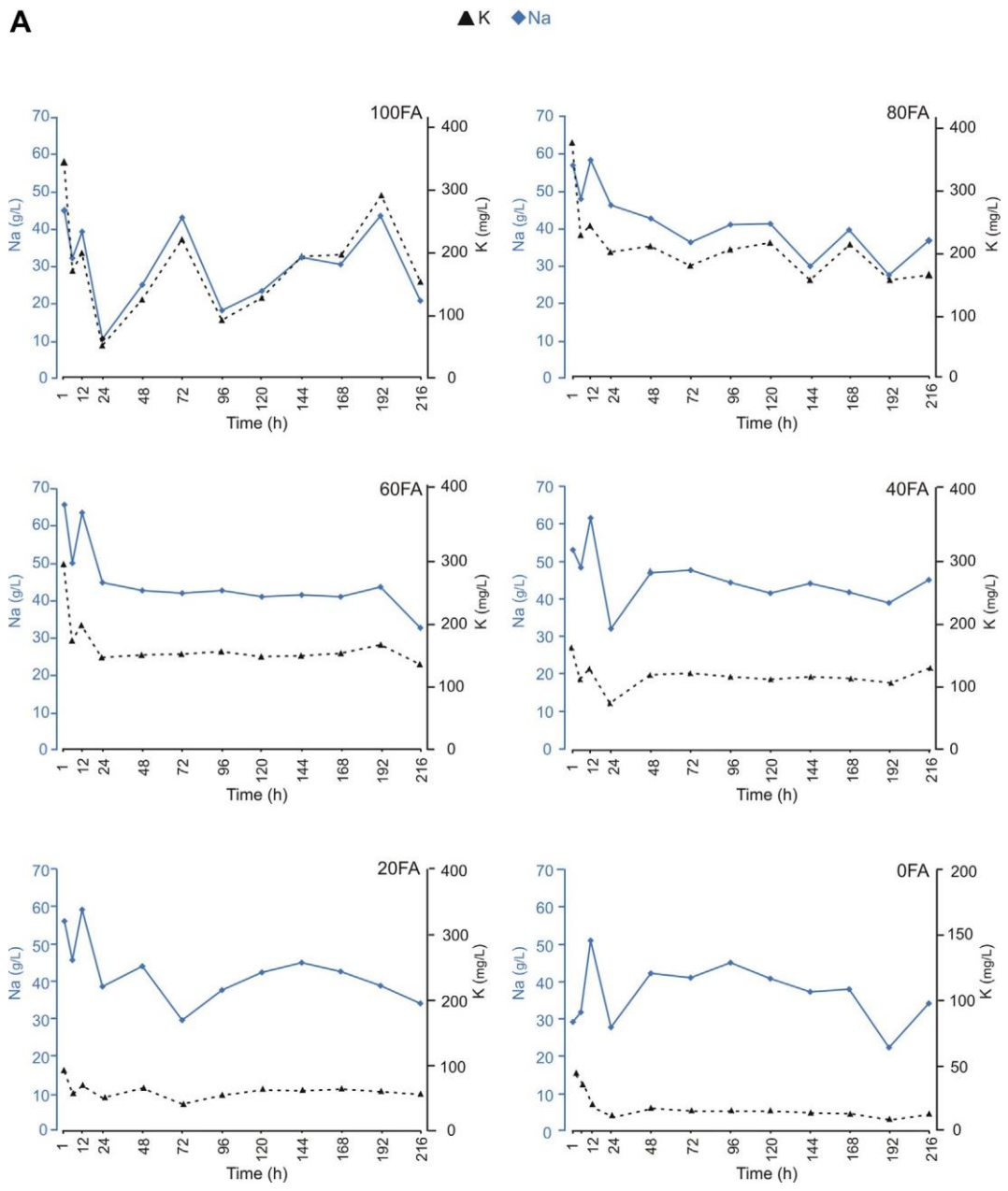

Fig. 3. Evolution of the Na and K (A), Ca and Mg (B) concentrations (mg/L) in the supernatant solutions over time.

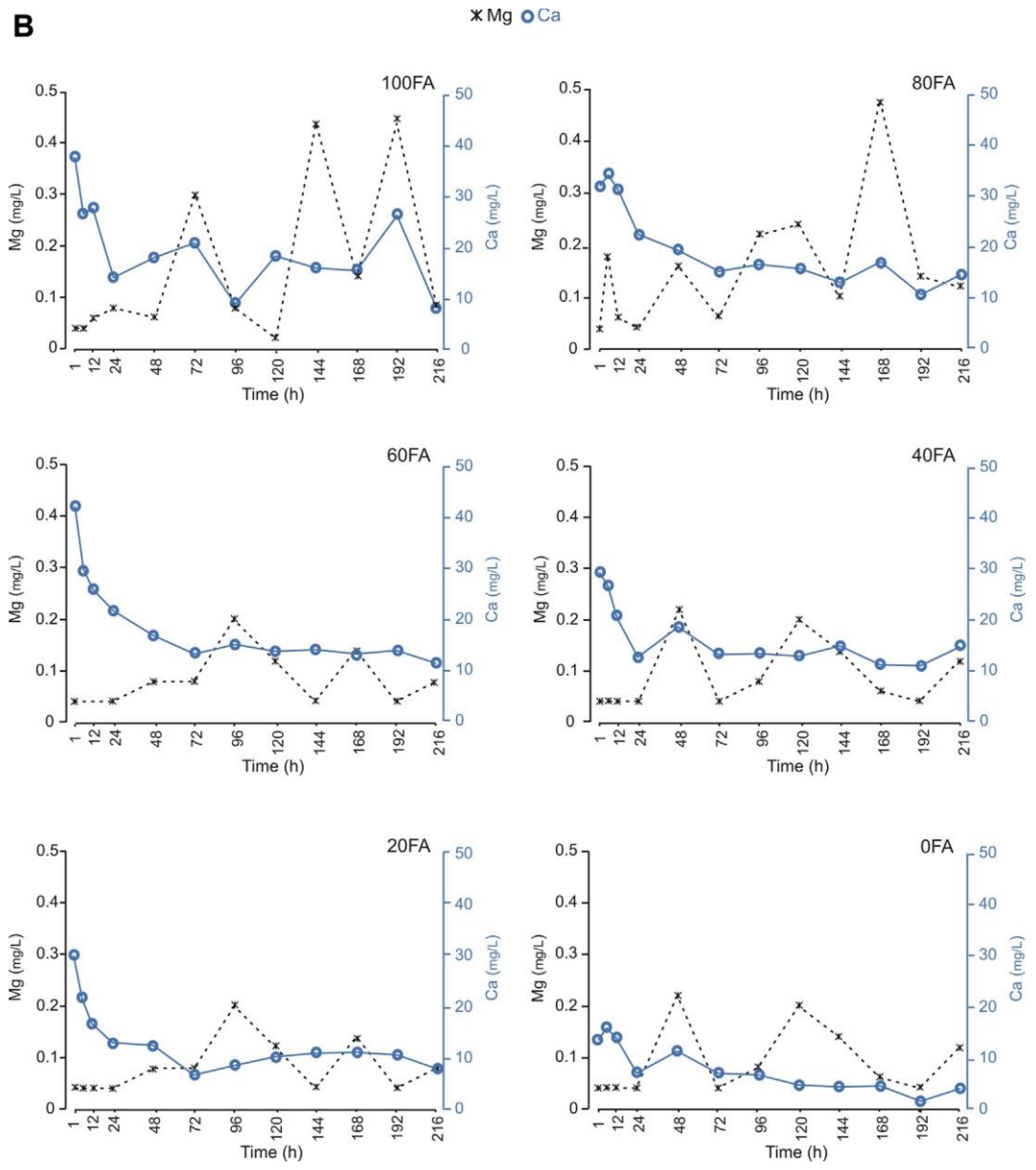

Fig. 3. (*continued*).

The Ca, K, Mg and Na concentrations in the supernatant solutions at different incubation times are reported in Table S1 and Fig. 3a and b. In detail, Ca_{aq} displayed a lower concentration in 0FA and higher concentrations in 80FA and 100FA, whereas K_{aq} was characterized by decreasing concentration from 100FA to 0FA and was detectable at each incubation time. Finally, Mg_{aq} was generally characterized by very low concentrations and a fluctuating behaviour in all of the samples, as did Na_{aq}.

4. Discussion

The XRD data (Figs. S3 and S4) confirmed what is already known in the literature (e.g., [9,10,13,14,16,19,31,36e38]): the Si/Al of the starting material exerts an important role on controlling the synthesis of the zeolitic phases. In this study, crystallization of the zeolite-X was favoured using fly

ash as starting material, whereas the A-type zeolite crystallized using KGa-2. However, the Si/Al ratio could not be considered the only factor controlling zeolite crystallization. In fact, if the four mixtures (with Si/Al values intermediate between those of FA and KGa-2) are considered (Fig. S4; Table 2), no gradual variations in the amounts of newly formed minerals were observed. The amount of zeolite-X tended to in- crease with the Si/Al ratio (up to Si/Al 1.35), and the zeolite-A concentration tended to decrease (Fig. 4); however, the two variables were not statistically correlated except in the samples incubated for 120 h (r^2 0.93) and 192 h (r^2 0.97). For a given Si/Al value, the amounts of the two minerals varied significantly depending on the duration of the experiment. This is apparent in Fig. 5 and Fig. S6, indicating that the amounts of zeolite-A and zeolite-X vary both over time and with the Si/Al value. The zeolite- X that formed in 100FA did not follow the trend outlined by the other five starting materials but was found in lower amounts from the trend depicted in Fig. 4. There is no simple explanation for this observation also because, as it will be showed below, there is a correlation between Si_{aq} and Al_{aq} concentrations and "amounts" of zeolite-X.

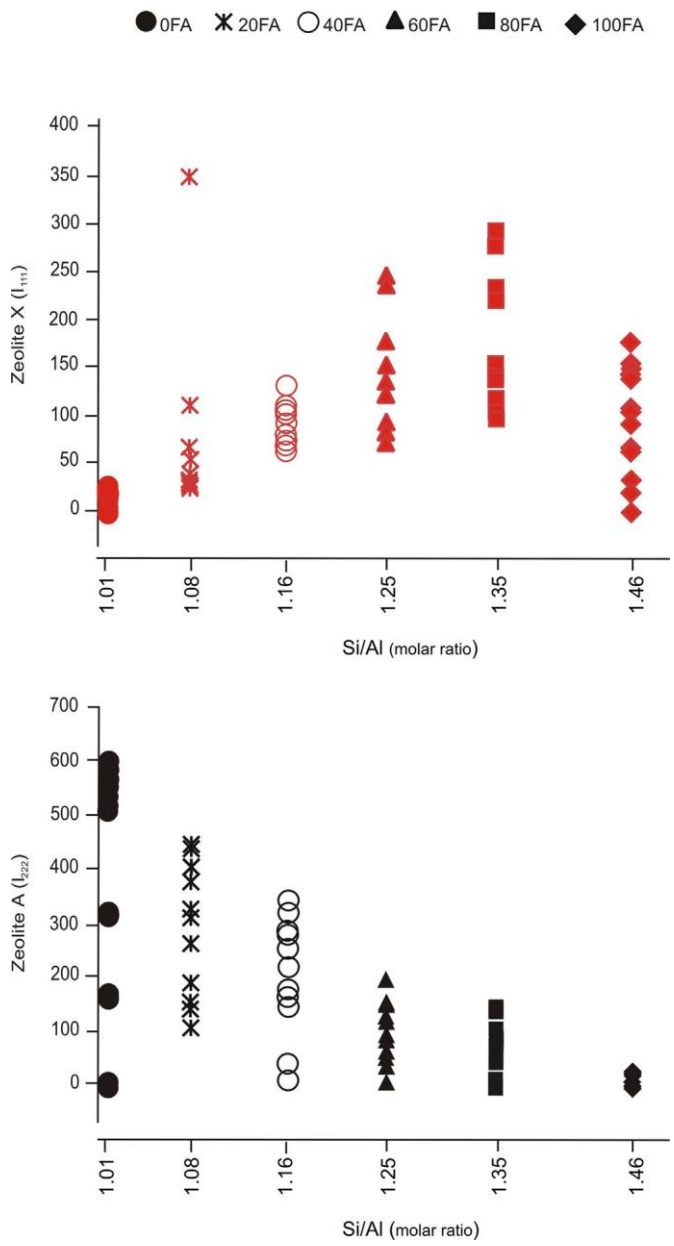

Fig. 4. Plot of the integrated intensities of the I_{222} and I_{111} diffraction lines for A-type and X-type zeolites, respectively, versus the Si/Al molar ratio of the starting material at different times.

Variations in the amounts of zeolite-A and zeolite-X in the products formed during the experiments could be related to the solubilization of the minerals because of their metastable behaviour, but it should be noted that a decrease in the amount of a phase at a given time does not correspond to an increase in the Si and Al concentrations in the solutions (Fig. 2). This behaviour has already been observed in a previous study on the

synthesis of zeolites from fly ash at room temperature (25 °C) in artificial seawater [11]. However, although some crystals exhibited traces of dissolution (p. 118; Fig. 4g and h), it was not possible to establish whether the minerals dissolved or amorphized; furthermore, a speculative hypothesis was formed suggesting detailing "*a continuous ion transfer from solid to solution (zeolites and geopolymers*

dissolution) and vice versa (precipitation/growth of zeolites and amorphous or poorly crystal- line solids)". Now, there is experimental evidence for this hypothesis that also provides a better understanding about the mechanisms governing the synthesis of zeolites. Amorphization implies changes in the geopolymer arrangement, and it can be derived by measuring the 2-theta position of the maximum in- tensity of the amorphous diffraction band. The results of these measurements are reported in Fig. 6. After 24 h (48 in the case of 100FA), the amorphous diffraction bands shifted approximately from 18°-40° 2θ to 20°-39° 2θ and, correspondingly, the maximum intensities move from about 29° 2θ (d ~ 0.31 nm) to about 32° 2θ (d ~ 0.28 nm), (thereby indicating the contraction of aluminosilicate gels. These values, however, varied over time, indicating that the average distances of the geopolymeric net-works changed during the experiments, likely because of crystallization/amorphization processes. However, it should be clearly stated that there is no correspondence between the variation in the maximum of the amorphous diffraction bands and the intensities of the zeolite-A and zeolite-X diffraction peaks. This is likely because the geopolymeric distances are influenced both by the zeolite crystallization/amorphization and by ion exchanges between the solid and solution. It should also be noted that the 100FA and 0FA trends differed significantly. These differences could be ascribed to their different Si/Al ratios and cations, but the presence of the residual AlO^{VI} (Fig. S5) might have played a role in determining the more stable 0FA geopolymer.

In accordance with previous studies (e.g., [11,19]), sodium silicate and sodium aluminosilicate formed after the alkaline fusion of kaolinite and fly ash. These compounds dissolved in distilled water, generating amorphous aluminosilicate gels that, after 24-48 h (Fig. 6), formed a shorter-range Si-Al network (geo- polymer). Except for calcium, which mainly participated in the formation of calcite, the concentrations of the other elements in the contact solutions decreased significantly during the first 24e48 h, thereby indicating that they participated in gel polymerization. After 48 h, decreasing trends were recorded, but the concentrations fluctuated over time, likely due to the precipitation/dissolution processes that accompanied mineral crystallization/amorphization. The distributions differed depending on the chemical composition of the starting material. It is interesting to note that the relative position of the Si_{aq} and Al_{aq} distribution patterns corresponds to the relative position of the distributions of zeolite-A and zeolite-X (Fig. 7): higher Si_{aq} corresponds to higher zeolite-X, and higher Al_{aq} corresponds to higher zeolite-A. As stated before, correlations among neoformed zeolites and the Si/Al ratio were not statistically significant, but we should compare the "amounts" of zeolite-A and -X with the Si_{aq} and Al_{aq} concentrations by excluding the experiments with incubation times shorter than 48 h. This is because the gel drastically changes in terms of the degree of polymerization during the initial 24 h as clearly indicated by the shift of the position of the maximum intensity of the amorphous diffraction band from 29°-30° 2θ to 31°-33° 2θ (Fig. 6); therefore, the neoformation of zeolites was strongly dependent on the local environmental conditions. The results of such a comparison (Fig. 8) confirmed the existence of statistically significant correlations: they were positive between the Si_{aq} and zeolite-X and between the Al_{aq} and zeolite-A; conversely, they were negative between the Si_{aq} and zeolite-A and

the Al_{aq} and zeolite-X.

Another important aspect to highlight is the behavior of Na and K. As expected, they had similar trends, and the concentration of potassium reflected the chemical composition of the starting materials (Fig. 3a). However, in spite of their geochemical affinity, Na is preferred to K (Fig. 9) in forming zeolites (e.g., [4]).

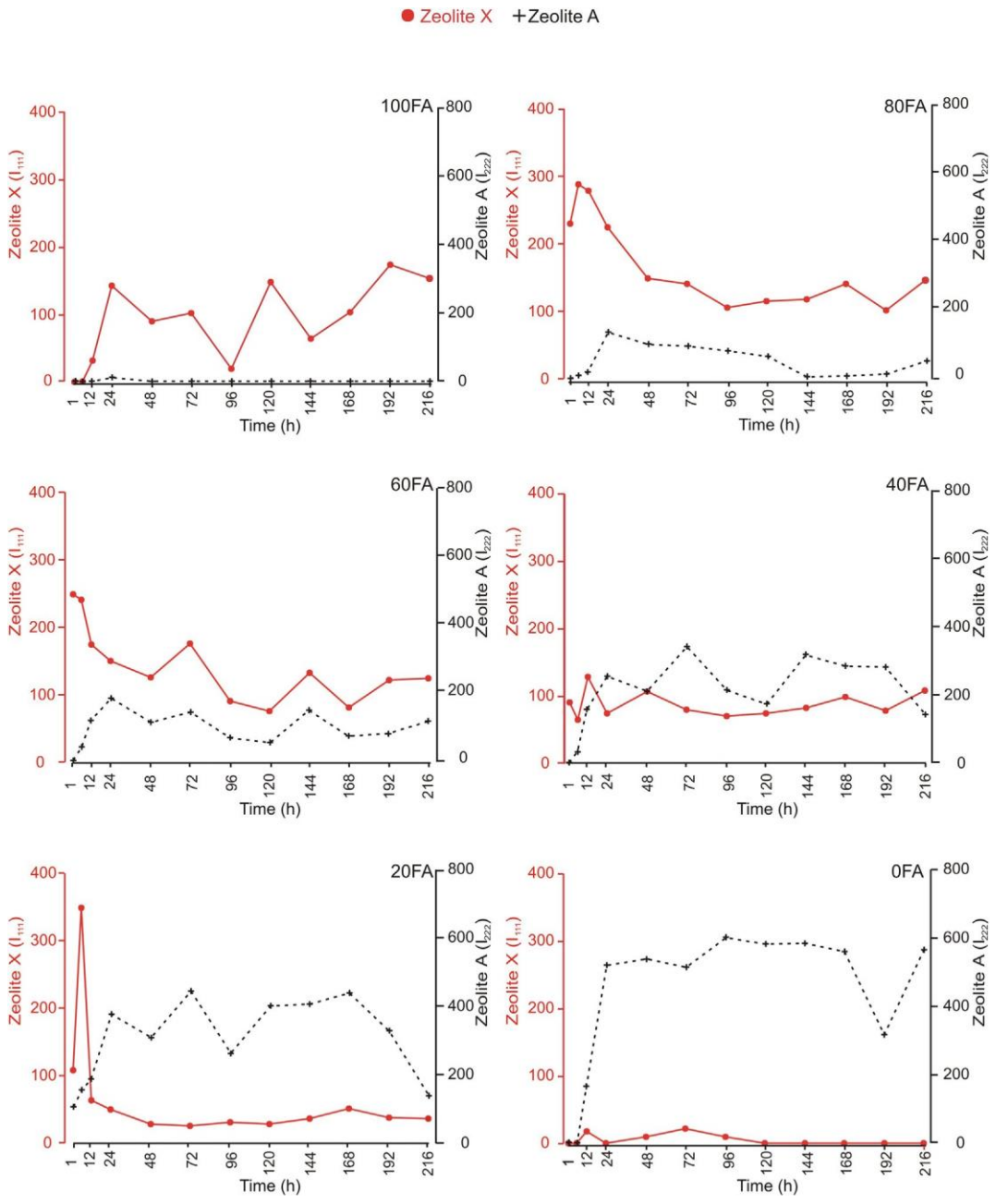

Fig. 5. Evolution of the integrated intensities of the I_{222} and I_{111} diffraction lines for A-type and X-type zeolites, respectively, over time.

EDS chemical analyses of gels incubated for 1 h indicated that their average Si/Al ratio was comparable to that of the starting material before alkaline fusion (max difference: 10%), but the values varied over a wide range, with the differences between the lowest and the highest values compared to

the initial ones as large as 50%. The inhomogeneous composition of geopolymeric materials, which changed during the experiments, could be the cause of the random sodalite crystallization, which occurs in all of the mixtures, irrespective of the incubation time, and of zeolite ZK-5, which crystallized in some experiments involving 100FA. In other words, the minerals formed where the geopolymer chemical composition was favourable to their formation.

5. Concluding remarks

Experiments using coal fly ash, kaolinite and their mixtures in distilled water at 45 °C were performed to obtain information regarding the factors that may play a role in controlling the crystallization of A-type and X-type zeolites at 45 °C using different types of source materials. The results indicate that, in addition to the Si/Al ratio of the starting materials, the synthesis of these minerals was driven by incubation times and the supernatant solution chemistry. The SEM-EDS analyses indicated that the Si/Al ratio of the geopolymers varies locally. It is likely that this variation determines the local chemical conditions favourable to the formation of other zeolitic phases, such as sodalite and ZK-5. The zeolites amounts changed during incubation. Because there is no chemical evidence of their dissolution, it has been suggested that they amorphized. This mechanism, together with ionic exchanges between gels and solutions, may be the cause of variation in the polymerization state of the alumino-silicate network over time. Sodalite and ZK-5 may form depending on the local favourable chemical composition of geopolymers.

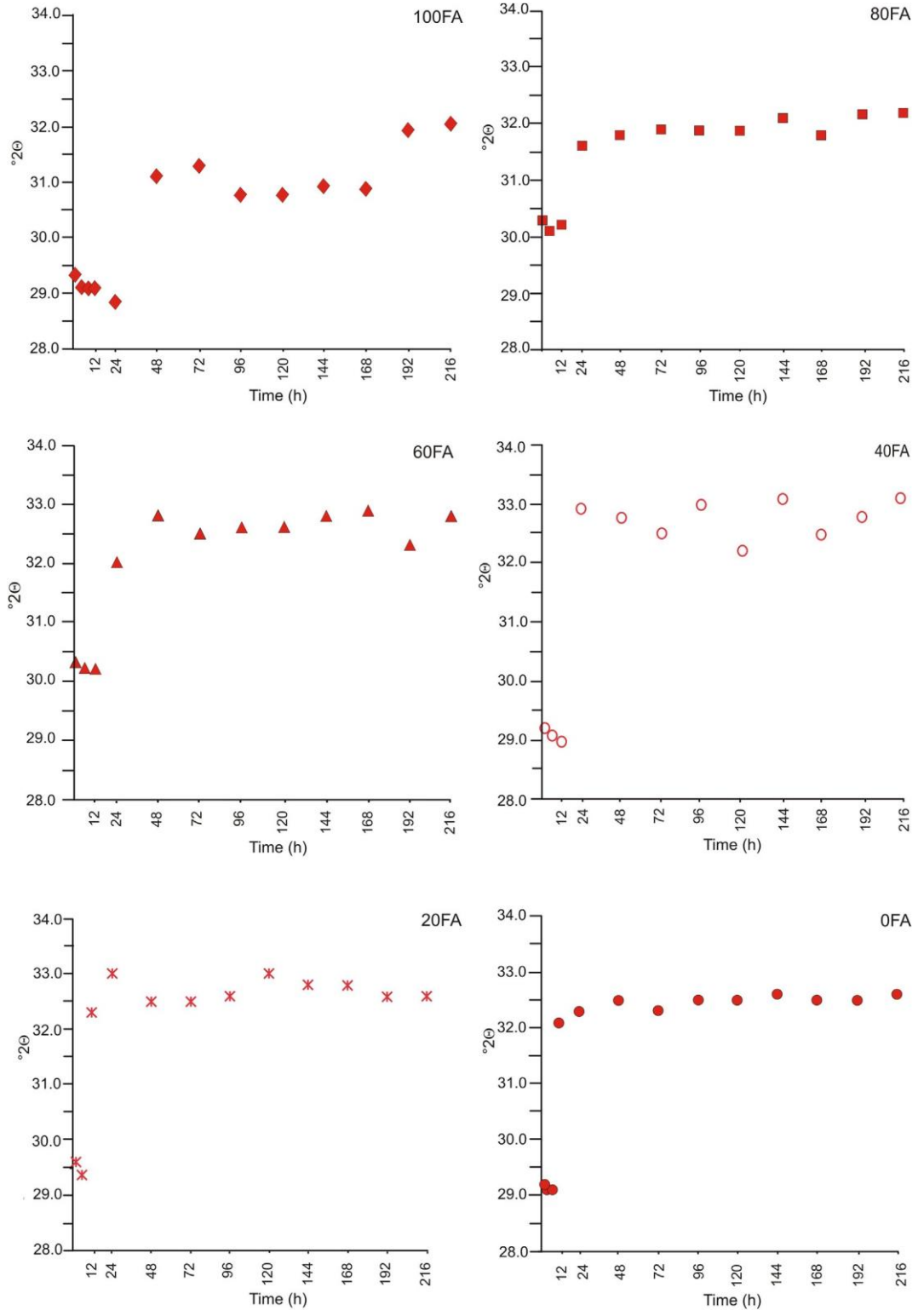

Fig. 6. Plot of the 2-theta position of maximum intensity of the amorphous diffraction band over time showing the "contraction" of the geopolymer after 24-48 h of incubation. Variations in the position of the band, i.e., "contraction-expansion" of the geopolymer network, may be partially due to the crystallization e amorphization of the zeolites.

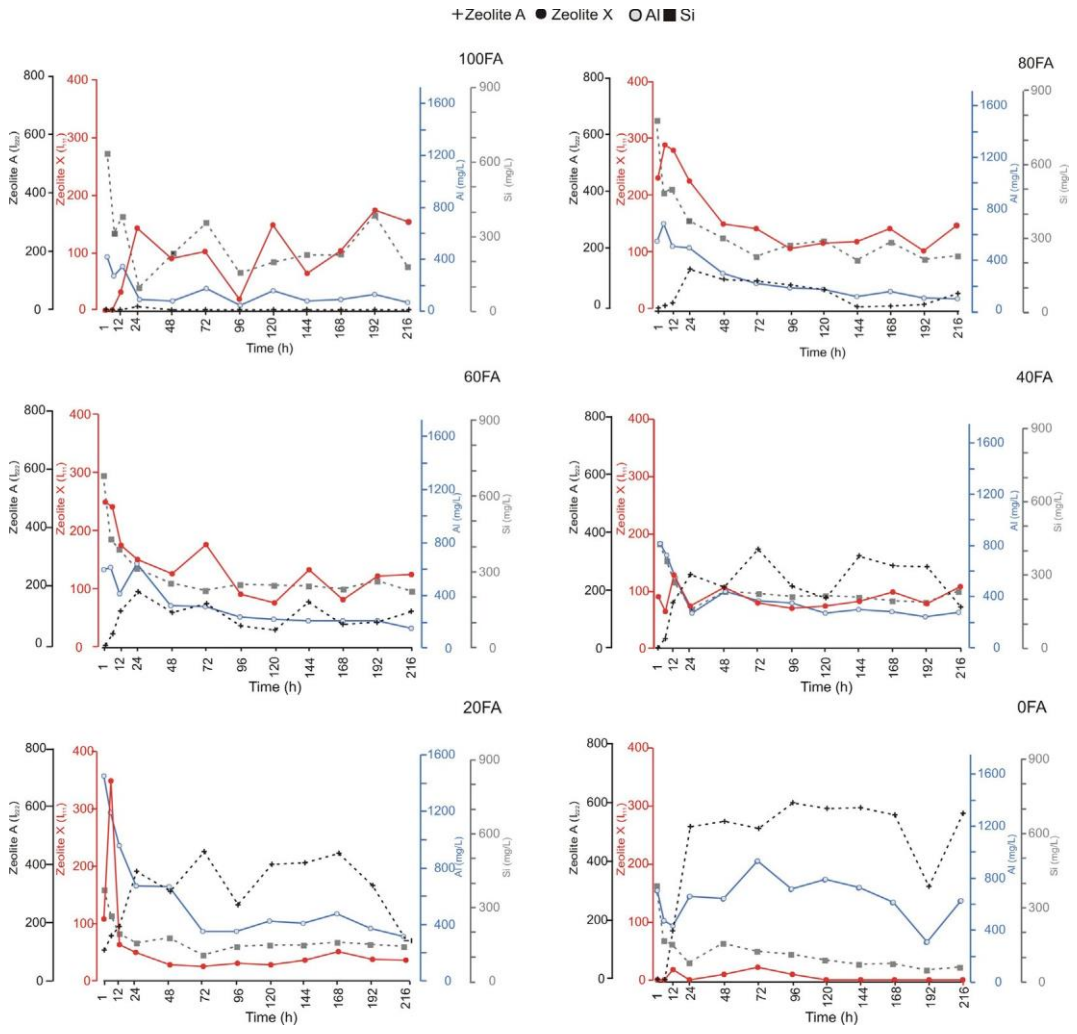

Fig. 7. Comparison of the Si and Al distributions (concentrations, in mg/L) in the supernatant solutions and the XRD intensity of zeolite-A and zeolite-X over time.

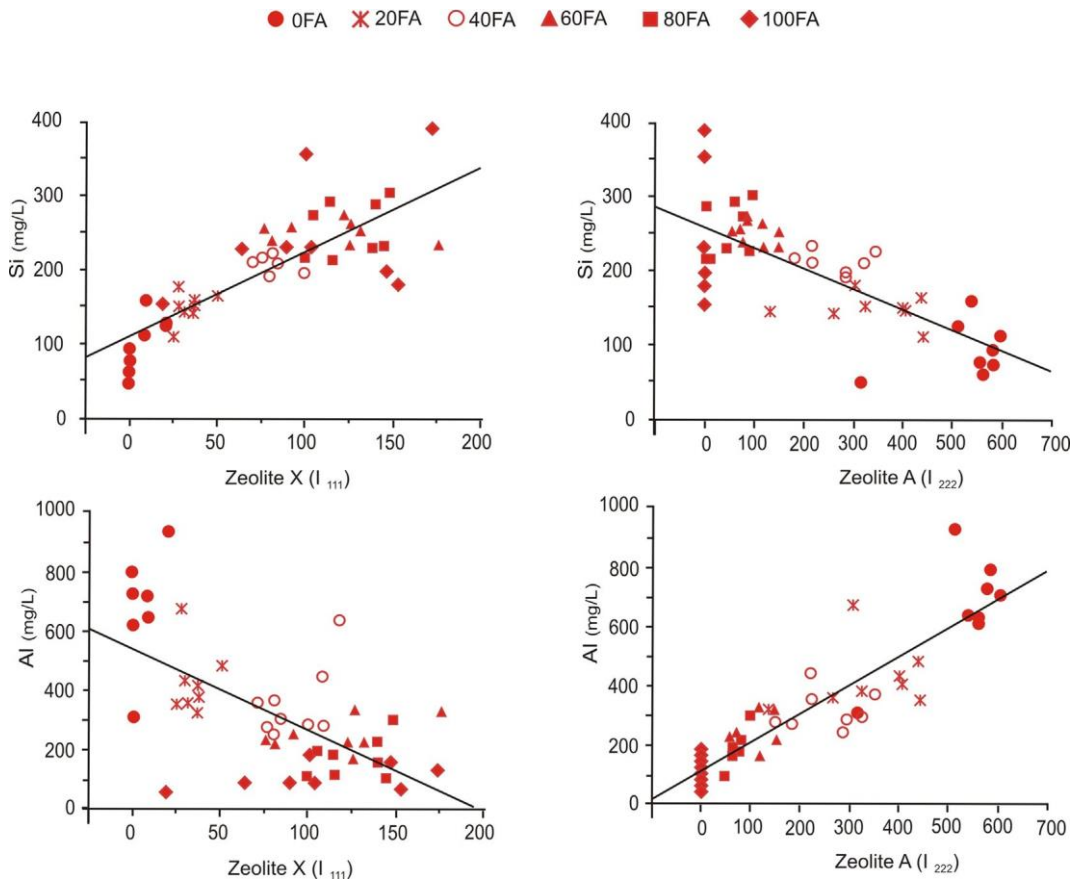

Fig. 8. Plot of the integrated intensities of the I_{222} and I_{111} diffraction lines for A-type and X-type zeolites, respectively, versus the Si and Al concentrations in the supernatant solutions. Data points for incubation times <48 h have been excluded (see text).

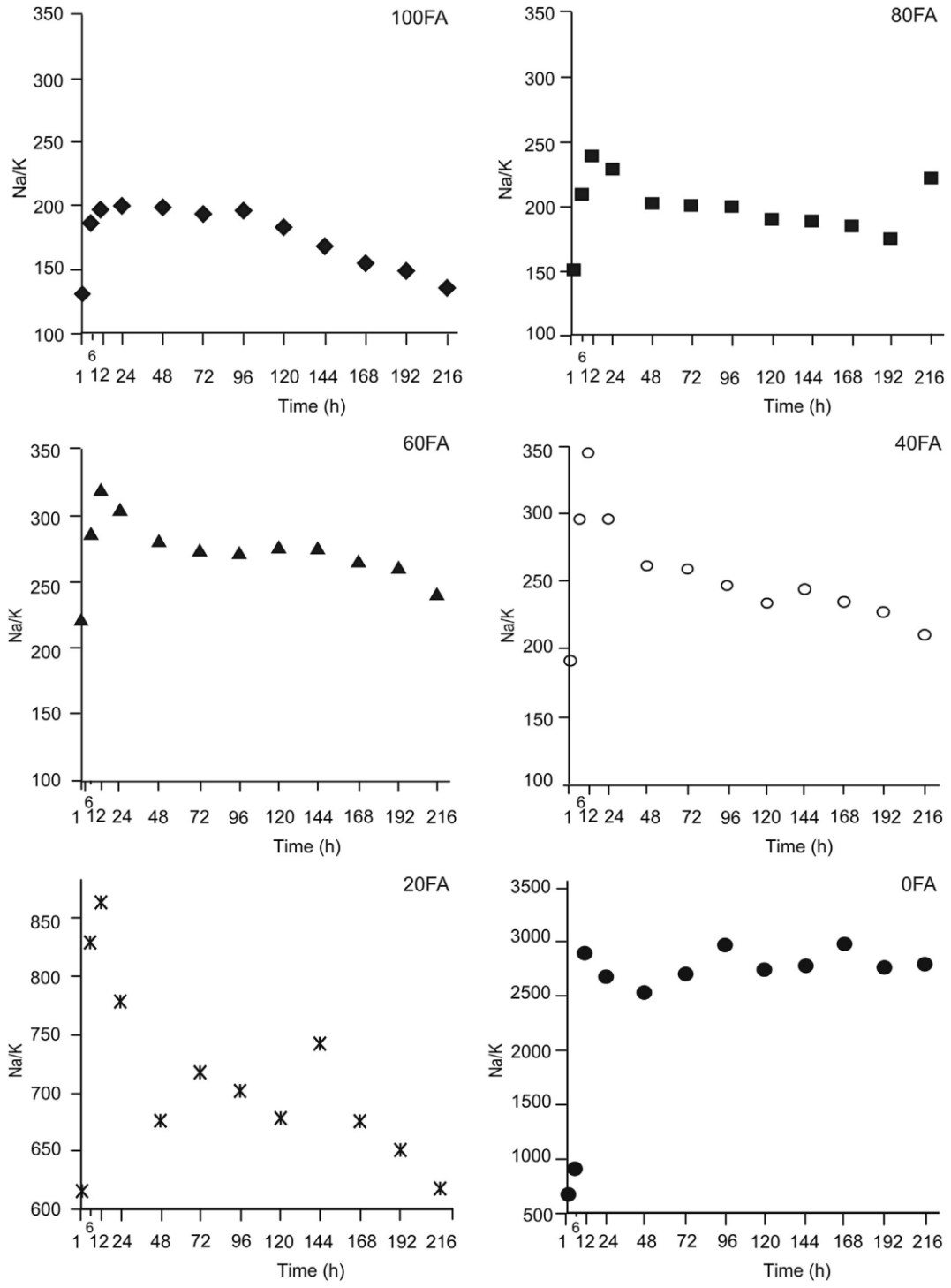

Fig. 9. Evolution of the Na/K molar ratio over time in the supernatant solutions.

Acknowledgements

We wish to thanks Prof. Piero Mastrorilli for the NMR analyses and suggestions. This study was partially financed by IMAA-CNR and the Italian Association for the Study of Clays (AISA).

6. References

[1] N. Shigemoto, H. Hayashi, K. Miyaura, J. Mater. Sci. 28 (1993) 4781-4786.

[2] V. Berkgaut, A. Singer, Appl. Clay Sci. 10 (1996) 369-378.

[3] X. Querol, A. Alastuey, F. Turiel, A. Lopez-Soler, Fuel 74 (1995) 1226-1231.

[4] X. Querol, F. Plana, A. Alastuey, A. Lopez-Soler, Fuel 76 (1997) 793-799.

[5] X. Querol, N. Moreno, J.C. Umaña, A. Alastuey, E. Hernandez, A. Lopez-Soler, F. Plana, Int. J. Coal Geol. 50 (2002) 413-423.

[6] H.L. Chang, W.H. Shih, Ind. Eng. Chem. Res. 37 (1998) 71-78.

[7] A. Molina, C.A. Poole, Min. Eng. 17 (2004) 167-173.

[8] M. Inada, Y. Eguchi, N. Enomoto, J. Hojo, Fuel 84 (2005) 299-304.

[9] C. Belviso, F. Cavalcante, S. Fiore, Waste Manage. 30 (2010) 839-847.

[10] C. Belviso, F. Cavalcante, A. Lettino, S. Fiore, Coal Comb. Gas. Prod. 2 (2010) 1-13.

[11] C. Belviso, F. Cavalcante, F.J. Huertas, A. Lettino, P. Ragone, S. Fiore, Microporous Mesoporous. Mater. 162 (2012) 115-121.

[12] M. Murat, A. Amokrane, J.P. Bastide, L. Montanaro, Clay Min. 27 (1992) 119-130.

[13] A. Gualtieri, P. Norby, G. Artioli, J. Hanson, Phys. Chem. Min. 24 (1997) 191-199.

[14] J. Park, B.C. Kim, S.S. Park, H.C. Park, J. Mater. Sci. Lett. 20 (2001) 531-533.

[15] L. Heller-Kallai, I. Lapides, Appl. Clay Sci. 35 (2007) 99-107.

[16] I. Lapides, L. Heller-Kallai, Appl. Clay Sci. 35 (2007) 94-98.

[17] C.A. Ríos, C.D. Williams, M.A. Fullen, Appl. Clay Sci. 2 (2009) 446-454.

[18] C. Du, H. Yang, Am. Mineral. 95 (2010) 741-746.

[19] C. Belviso, F. Cavalcante, A. Lettino, S. Fiore, Appl. Clay Sci. 80-81 (2013) 162-168.

[20] P.M. Slangen, J.C. Jansen, H. van Bekkum, Microporous Mater. 9 (1997) 259-265.

[21] H. Katsuki, S. Futura, S. Komarneni, J. Porous Mater. (2001) 5-12.

[22] O. Andac, M. Tather, A. Sirkecioglu, I. Ece, A. Erdem-Senatalar, Microporous Mesoporous Mater. 79 (2005) 225-233.

[23] J.B. Wu, B.Y. Wang, N. Li, S.H. Xiang, Chin. J. Catal. 27 (2006) 375-377.

[24] B. Wang, J. Wu, Z.-Y. Yuan, N. Li, S. Xiang, Ultrason. Sonochem 15 (2008) 334-338.

[25] C. Belviso, F. Cavalcante, A. Lettino, S. Fiore, Ultrason. Sonochem 18 (2011) 661-668.

[26] C. Belviso, F. Cavalcante, S. Fiore, Ultrason. Sonochem 20 (2013b) 32-36.

[27] M. Yusoff, M. Masilana, T.F. Choo, A.M. Julie, Adv. Mater. Res. 30 (2007) 187-190.

[28] J.-Q. Wang, Y.-X. Huang, Y. Pan, J.-X. Mi, Micropor. Mesopor. Mat. 199 (2014) 50-56.

[29] J.R. Ugal, K.H. Hassan, I.H. Ali, J. Assoc. Arab. Univ. Basic Appl. Sci. 9 (2010) 2-5.

[30] M. Alkan, C. Hopa, Z. Yilmaz, H. Guler, Micropor. Mesopor. Mat. 86 (2005) 176-184.

[31] S. Chandrasekhar, Clay Miner. 31 (1996) 253-261.

[32] C.A. Rios, C.D. Williams, M.A. Fullen, Appl. Clay Sci. 42 (2009) 446-454.

[33] M. Kazemimoghadam, T. Mohammadi, Sep. Purif. Technol. 7 (2006) 173-178.

[34] I. Caballero, F.G. Colina, J. Costa, Ind. Eng. Chem. Res. 46 (2007) 1029e1038.

[35] C.S. Cundy, P.A. Cox, Microporous Mesoporous Mater. 82 (2005) 1e78.
[36] F. Mondragon, F. Rincon, L. Sierra, J. Escobar, J. Ramirez, J. Fernandez, Fuel 69 (1990) 263-266.
[37] G.G. Hollman, G. Steenbruggen, M. Janssen-Jurkovicova, Fuel 78 (1999) 1225-1230.
[38] L.V.C. Rees, S. Chandrasekhar, Zeolites 13 (1993) 524-533.

Appendix A. Supplementary data

Supplementary data related to this article can be found at http://dx.doi.org/10.1016/j.micromeso.2015.03.012.